Nonequilibrium Cation Distribution, Canted Spin Arrangement, and Enhanced Magnetization in Nanosized $MgFe_2O_4$ Prepared by a One-Step Mechanochemical Route

Vladimir Šepelák*,†

Center for Solid State Chemistry and New Materials, University of Hannover, Callinstrasse 3-3A, D-30167 Hannover, Germany

Armin Feldhoff and Paul Heitjans

Institute of Physical Chemistry and Electrochemistry, University of Hannover, Callinstrasse 3-3A, D-30167 Hannover, Germany

Frank Krumeich

Laboratory of Inorganic Chemistry, Swiss Federal Institute of Technology Zürich, Hönggerberg HCI-G105, CH-8093 Zurich, Switzerland

Dirk Menzel and Fred Jochen Litterst

Institute of Condensed Matter Physics, Braunschweig University of Technology, Mendelssohnstrasse 3, D-38106 Braunschweig, Germany

Ingo Bergmann and Klaus Dieter Becker

Institute of Physical and Theoretical Chemistry, Braunschweig University of Technology, Hans-Sommer-Strasse 10, D-38106 Braunschweig, Germany

Received July 10, 2005. Revised Manuscript Received April 18, 2006

A single-step synthesis of magnesium ferrite ($MgFe_2O_4$) nanoparticles with an average crystallite size of about 8.5 nm synthesized via mechanochemical processing of binary oxide precursors at room temperature is reported. The study highlights the nature of the cation disorder and of the spin arrangement in mechanosynthesized $MgFe_2O_4$ as well as its response to changes in temperature. An unusual property of the magnetization enhancement in nanoscale mechanosynthesized $MgFe_2O_4$ is reported. Whereas the inner core of a $MgFe_2O_4$ nanoparticle exhibits a partly inverse spinel structure with a Néel type collinear spin alignment, the major features of the ionic and spin configurations in the grain boundary (surface) region are a nonequilibrium cation distribution and a canted spin arrangement. Although the spin-canting effect tends to reduce the magnetic moment, the magnetization enhancement exhibited by mechanosynthesized $MgFe_2O_4$ is attributed to the nearly random distribution of magnetic cations in the surface regions of nanoparticles. On heating above 623 K, the mechanosynthesized $MgFe_2O_4$ relaxes to a structural and magnetic state that is similar to the bulk one.

Introduction

Nanosized spinel type ferrites are currently key materials for advancements in electronics, magnetic storage, ferrofluid technology, and many bioinspired applications (for example, as drug carriers for magnetically guided drug delivery and as contrast agents in magnetic resonance imaging).[1,2] Magnesium ferrite, $MgFe_2O_4$, as a soft magnetic *n*-type semiconducting material, is an important member of the spinel family. Apart from its magnetic and electronic applications,[3] $MgFe_2O_4$ finds a number of applications in heterogeneous catalysis and adsorption[4,5] and in sensor technology.[6] Recently, it has been demonstrated that this material can be used for thermal coagulation therapy, in which tumors are locally heated by an application of alternating magnetic fields.[7]

* To whom correspondence should be addressed. Tel: 49-531-3915341. Fax: 49-531-3917305. E-mail: v.sepelak@tu-bs.de.

† On leave from the Slovak Academy of Sciences, Watsonova 45, SK-04353 Košice, Slovakia.

(1) Wang, Z. L.; Liu, Y.; Zhang, Z. *Handbook of Nanophase and Nanostructured Materials. Vol. 3*; Kluwer Academic/Plenum Publishers: New York, 2002.

(2) Valenzuela, R. *Magnetic Ceramics*; Cambridge University Press: Cambridge, 1994.

(3) Goldman, A. *Modern Ferrite Technology*; Van Nostrand Reinhold: New York, 1990.

(4) Zhang, H.; Qi, R.; Evans, D. G.; Duan, X. *J. Solid State Chem.* **2004**, *177*, 772.

(5) Molchanov, V. V.; Buyanov, R. A.; Pavlyukhin, Y. T. *Kinet. Catal.* **2003**, *44*, 788.

(6) (a) Chen, N. S.; Yang, X. J.; Liu, E. S.; Huang, J. L. *Sens. Actuators, B* **2000**, *66*, 178. (b) Liu, Y. L.; Liu, Z. M.; Yang, Y.; Yang, H. F.; Shen, G. L.; Yu, R. Q. *Sens. Actuators, B* **2005**, *107*, 600.

10.1021/cm0514894 CCC: $33.50
Published on Web 05/25/2006

Magnesium ferrite bulk material is known to be a ferrimagnetic ternary oxide that crystallizes with the cubic spinel type structure ($a = 0.83998$ nm, space group $Fd\bar{3}m$; JCPDS PDF 88-1943).[8] To emphasize the site occupancy at the atomic level, we may write $MgFe_2O_4$ as $(Mg_{1-\lambda}Fe_{\lambda})[Mg_{\lambda}Fe_{2-\lambda}]O_4$, where parentheses and square brackets denote cation sites of tetrahedral (A) and octahedral [B] coordination, respectively. λ represents the so-called degree of inversion (defined as the fraction of the (A) sites occupied by Fe^{3+} cations). It is widely appreciated that the cation distribution in $MgFe_2O_4$, upon which many physical and chemical properties depend, is a complex function of processing parameters and depends on the preparation method of the material.[9]

Technological and scientific challenges coupled with environmental considerations have prompted a search for simple and energy-efficient synthesis and processing routes of nanocrystalline spinel ferrites.[10] Among the many types of preparation and processing techniques (including, for example, hydrothermal reactions,[11] coprecipitation,[12] combustion synthesis,[13] the sol−gel method,[14] microwave processing,[15] microemulsion procedures,[16] and sonochemical synthesis[17]), the nonconventional mechanochemical route[18] has been recognized as a powerful method for the production of novel, high-performance, and low-cost materials. The mechanochemical synthesis (mechanosynthesis) can deliver the designed phases and structures by a single step of the high-energy milling conducted in an enclosed activation chamber at room temperature.[19] In recent years, a surge of investigations in the field of mechanochemistry has resulted in the mechanosynthesis of stoichiometric and chemically pure nanoscale spinel ferrites such as $CoFe_2O_4$,[20] $MnFe_2O_4$,[21] $ZnFe_2O_4$,[18,22] Mn−Zn ferrites,[23] $Co_{0.2}Zn_{0.8}Fe_2O_4$,[24] $Ti_{0.5}Fe_{2.5}O_4$,[25] and $NiFe_2O_4$.[26] In some cases, complete formation of spinel ferrites was obtained only after milling followed by sintering, i.e., by employing two processing steps. It is obvious that the combined mechanochemical−thermal treatment yielded a well-ordered spinel phase in ferrites at lower annealing temperatures and shorter durations than those required in conventional ceramic methods.[27] In this article, we will report on the single-step synthesis of $MgFe_2O_4$ via high-energy milling of binary oxide precursors. To the best of our knowledge, the single-step mechanosynthesis of nanosized $MgFe_2O_4$ particles has not been reported before. Previous attempts to synthesize $MgFe_2O_4$ from the powdered precursors in a ball mill led only to the partial conversion to $MgFe_2O_4$.[28] It was largely due to the choice of the relatively mild synthesis conditions, represented mainly by the mass of the balls, which strongly influences the impact energies and, consequently, the yield of a mechanochemical reaction.

It should be emphasized that in most of the above-mentioned papers on mechanosynthesis of spinel ferrites, only the formation of mechanosynthesized oxides has been established by X-ray diffraction and/or Mössbauer spectroscopy. Not much work has been done to determine the defect state or the structure of oxides prepared by nonconventional mechanochemical routes. Especially, the evaluation of the cation distribution in mechanosynthesized spinel ferrites from Mössbauer spectra and/or X-ray diffraction patterns is not

(7) (a) Maehara, T.; Konishi, K.; Kamimori, T.; Aono, H.; Hirazawa, H.; Naohara, T.; Nomura, S.; Kikkawa, H.; Watanabe, Y.; Kawachi, K. *J. Mater. Sci.* **2005**, *40*, 135. (b) Konishi, K.; Maehara, T.; Kamimori, T.; Aono, H.; Naohara, T.; Kikkawa, H.; Watanabe, Y.; Kawachi, K. *J. Magn. Magn. Mater.* **2004**, *272−276*, 2428.

(8) *Joint Committee on Powder Diffraction Standards (JCPDS) Powder Diffraction File (PDF)*; International Centre for Diffraction Data: Newtown Square, PA, 2004.

(9) (a) O'Neill, H. S. C.; Annersten, H.; Virgo, D. *Am. Mineral.* **1992**, *77*, 725. (b) Šepelák, V.; Schultze, D.; Krumeich, F.; Steinike, U.; Becker, K. D. *Solid State Ionics* **2001**, *141−142*, 677. (c) Wang, Z.; Lazor, P.; Saxena, S. K.; O'Neill, H. S. C. *Mater. Res. Bull.* **2002**, *37*, 1589. (d) Levy, D.; Diella, V.; Dapiaggi, M.; Sani, A.; Gemmi, M.; Pavese, A. *Phys. Chem. Miner.* **2004**, *31*, 122.

(10) Willard, M. A.; Kurihara, L. K.; Carpenter, E. E.; Calvin, S.; Harris, V. G. *Int. Mater. Rev.* **2004**, *49*, 125.

(11) (a) Yu, S. H.; Yoshimura, M. *Chem. Mater.* **2000**, *12*, 3805. (b) Wang, H. W.; Kung, S. C. *J. Magn. Magn. Mater.* **2004**, *270*, 230.

(12) (a) Lechevallier, L.; Le Breton, J. M.; Wang, J. F.; Harris, I. R. *J. Phys.: Condens. Matter* **2004**, *16*, 5359. (b) Shenoy, S. D.; Joy, P. A.; Anantharaman, M. R. *J. Magn. Magn. Mater.* **2004**, *269*, 217. (c) Nivoix, V.; Gillot, B. *Chem. Mater.* **2000**, *12*, 2971.

(13) Hwang, C. C.; Tsai, J. S.; Huang, T. H.; Peng, C. H.; Chen, S. Y. *J. Solid State Chem.* **2005**, *178*, 382.

(14) (a) Veith, M.; Haas, M.; Huch, V. *Chem. Mater.* **2005**, *17*, 95. (b) Chakraverty, S.; Mandal, K.; Mitra, S.; Chattopadhyay, S.; Kumar, S. *Jpn. J. Appl. Phys.* **2004**, *43*, 7782. (c) Silva, M. N. B.; Duque, J. G. D.; Gouveia, D. X.; de Paiva, J. A. C.; Macedo, M. A. *Jpn. J. Appl. Phys.* **2004**, *43*, 5249.

(15) (a) Komarneni, S.; D'Arrigo, M. C.; Leonelli, C.; Pellacani, G. C.; Katsuki, H. *J. Am. Ceram. Soc.* **1998**, *81*, 3041. (b) Verma, S.; Joy, P. A.; Khollam, Y. B.; Potdar, H. S.; Deshpande, S. B. *Mater. Lett.* **2004**, *58*, 1092.

(16) (a) Vestal, C. R.; Zhang, Z. J. *Chem. Mater.* **2002**, *14*, 3817. (b) Grasset, F.; Labhsetwar, N.; Li, D.; Park, D. C.; Saito, N.; Haneda, H.; Cador, O.; Roisnel, T.; Mornet, S.; Duguet, E.; Portier, J.; Etourneau, J. *Langmuir* **2002**, *18*, 8209.

(17) Baranchikov, A. E.; Ivanov, V. K.; Oleinikov, N. N.; Tret'yakov, Y. D. *Inorg. Mater.* **2004**, *40*, 1091.

(18) Šepelák, V.; Steinike, U.; Uecker, D. C.; Wissmann, S.; Becker, K. D. *J. Solid State Chem.* **1998**, *135*, 52.

(19) Avvakumov, E.; Senna, M.; Kosova, N. *Soft Mechanochemical Synthesis: A Basis for New Chemical Technologies*; Kluwer Academic Publishers: Boston, 2001.

(20) Manova, E.; Kunev, B.; Paneva, D.; Mitov, I.; Petrov, L.; Estournès, C.; D'Orléans, C.; Rehspringer, J.-L.; Kurmoo, M. *Chem. Mater.* **2004**, *16*, 5689.

(21) (a) Muroi, M.; Street, R.; McCormick, P. G.; Amighian, J. *Phys. Rev. B* **2001**, *63*, 184414. (b) Padella, F.; Alvani, C.; La Barbera, A.; Ennas, G.; Liberatore, R.; Varsano, F. *Mater. Chem. Phys.* **2005**, *90*, 172. (c) Osmokrović, P.; Jovalekić, Č.; Manojlović, D.; Pavlović, M. B. *J. Optoelectron. Adv. Mater.* **2006**, *8*, 312.

(22) (a) Druska, P.; Steinike, U.; Šepelák, V. *J. Solid State Chem.* **1999**, *146*, 13. (b) Šepelák, V.; Wissmann, S.; Becker, K. D. *J. Magn. Magn. Mater.* **1999**, *203*, 135. (c) Goya, G. F.; Rechenberg, H. R.; Chen, M.; Yelon, W. B. *J. Appl. Phys.* **2000**, *87*, 8005. (d) Kim, W.; Saito, F. *Powder Technol.* **2001**, *114*, 12. (e) Bid, S.; Pradhan, S. K. *Mater. Chem. Phys.* **2003**, *82*, 27. (f) Verdier, T.; Nachbaur, V.; Jean, M. *J. Solid State Chem.* **2005**, *178*, 3243.

(23) (a) Harris, V. G.; Fatemi, D. J.; Cross, J. O.; Carpenter, E. E.; Browning, V. M.; Kirkland, J. P.; Mohan, A.; Long, G. J. *J. Appl. Phys.* **2003**, *94*, 496. (b) Verdier, T.; Nivoix, V.; Jean, M.; Hannoyer, B. *J. Mater. Sci.* **2004**, *39*, 5151.

(24) Bhowmik, R. N.; Ranganathan, R. *J. Mater. Sci.* **2002**, *37*, 4391.

(25) Guigue-Millot, N.; Begin-Colin, S.; Champion, Y.; Hytch, M. J.; Le Caër, G.; Perriat, P. *J. Solid State Chem.* **2003**, *170*, 30.

(26) (a) Šepelák, V.; Menzel, M.; Bergmann, I.; Wiebcke, M.; Krumeich, F.; Becker, K. D. *J. Magn. Magn. Mater.* **2004**, *272−276*, 1616. (b) Yang, H.; Zhang, X.; Ao, W.; Qiu, G. *Mater. Res. Bull.* **2004**, *39*, 833. (c) Zhou, Z. H.; Xue, J. M.; Wang, J.; Chan, H. S. O.; Yu, T.; Shen, Z. X. *J. Appl. Phys.* **2002**, *91*, 6015.

(27) (a) Yang, H. M.; Zhang, X. C.; Tang, A. D.; Qiu, G. Z. *Chem. Lett.* **2004**, *33*, 826. (b) Ennas, G.; Marongiu, G.; Marras, S.; Piccaluga, G. *J. Nanopart. Res.* **2004**, *6*, 99. (c) Bid, S.; Pradhan, S. K. *Jpn. J. Appl. Phys.* **2004**, *43*, 5455. (d) Mozaffari, M.; Amighian, J. *J. Magn. Magn. Mater.* **2003**, *260*, 244. (e) Widatallah, H. M.; Berry, F. J. *J. Solid State Chem.* **2002**, *164*, 230.

(28) (a) Moustafa, S. F.; Morsi, M. B. *Mater. Lett.* **1998**, *34*, 241. (b) Huerta, A.; Calderon, H. A.; Umemoto, M. *Mater. Sci. Forum* **2001**, *360−362*, 631. (c) Rabanal, M. E.; Várez, A.; Levenfeld, B.; Torralba, J. M. *Mater. Sci. Forum* **2003**, *426−432*, 4349.

as straightforward as is frequently claimed in the literature. The hyperfine interactions in (A) and [B] sites of a nanoscale spinel ferrite usually do not differ substantially and possess a more or less distributive character.[29] Under these conditions, it can happen that the (A) and [B] Mössbauer subspectra are difficult to resolve because of strongly overlapping lines. This is clearly demonstrated in the case of mechanosynthesized $CoFe_2O_4$,[20] in which an unusual cation distribution was derived from Mössbauer spectra with strongly overlapping lines. According to our experience,[29,30] the use of both large external magnetic fields and low temperatures is indispensable in many cases in order to allow for a unanimous separation of the contributions from both sites. Thus, cation distributions merely determined from Mössbauer spectra without application of an external magnetic field have to be considered with reserve, especially when conclusions are drawn from spectra with low resolution or bad statistics.

Because of their sensitivity to medium- and long-range structural order, diffraction techniques also lose much of their resolving power in nanoscale systems. Despite this fact, Pradhan et al.[31] have recently attempted to obtain information about the cation distribution in mechanosynthesized $MgFe_2O_4$ nanoparticles using Rietveld analysis of the X-ray diffraction data. It has been shown that the mechanosynthesized material consists of two spinel phases with different cation distributions (mixed spinel and inverse spinel). However, the precise quantitative estimates of the degrees of inversion of these phases are prohibited because the X-ray atomic scattering factors of magnesium and iron cations (which are proportional to the number of electrons) don't differ sufficiently enough to allow an accurate evaluation of the cation distribution in $MgFe_2O_4$ nanoparticles. In this article, we present a detailed study of the ionic and spin arrangement in nanosized mechanosynthesized $MgFe_2O_4$. For the first time, quantitative microstructural information is obtained on both the nonequilibrium cation distribution and the noncollinear spin arrangement in nanosized $MgFe_2O_4$ synthesized in a one-step mechanochemical process.

The scientific importance of synthesizing functional nanoparticles lies in the fact that they exhibit numerous new properties. In the present paper, we also demonstrate that nanoscale mechanosynthesized $MgFe_2O_4$ possesses an enhanced saturation magnetization, attaining a value approximately 50% larger than that of bulk $MgFe_2O_4$. It should be emphasized that there is only a limited number of studies on the enhancement of magnetic properties in mechanochemically prepared spinel ferrites.[22b,30,32] As reported in the majority of studies on the magnetic behavior of ionic magnetic solids, their particle size reduction to nanometer scale leads to a reduced magnetization and ordering temperature and an increased anisotropy.[21a,26a] The origin of the observed "magnetic degradation" in fine magnetic particles is often connected with the existence of a "magnetically dead" layer at the particle surface[21a] and is discussed in terms of the core−shell exchange-coupling model proposed by Kodama and co-workers.[33]

Another problem, which is treated only to a limited extent in the literature, is related to the thermal stability of mechanochemically prepared spinel ferrites, which are often inherently unstable because of their small constituent sizes, disordered structural state, and high chemical activity.[34] In the present work, the response of nanoscale mechanosynthesized $MgFe_2O_4$ to changes in temperature is also studied. This is of importance not only for basic science but also because of possible high-temperature applications of mechanosynthesized ferrites.[34d]

Experimental Section

The mechanochemical route was used for the preparation of nanostructured $MgFe_2O_4$. Stoichiometric mixtures of α-Fe_2O_3 and MgO reactants (Merck, Darmstadt, Germany) were used as starting materials. The starting mixtures (10 g) were milled for various uninterrupted times (up to 12 h) in a Pulverisette 6 planetary ball mill (Fritsch, Idar-Oberstein, Germany) at room temperature. A grinding chamber (250 cm^3 in volume) and balls (10 mm in diameter) made of tungsten carbide were used. The ball-to-powder weight ratio was 20:1. Milling experiments were performed in air at 600 rpm.

Additionally, bulk $MgFe_2O_4$, which served as a reference sample in this study, was prepared from equimolar amounts of reagent-grade oxides (α-Fe_2O_3 and MgO) by the conventional solid-state route. Powdered reactants were, at first, homogenized under ethanol in an agate mortar and then pressed into tablets (20 mm in diameter, 4 mm thick) under a pressure of 30 MPa in a steel mold in order to obtain a high degree of compaction. The reaction tablets were prefired twice at 1200 K for 24 h, reground, pressed, and finally sintered at 1300 K for 24 h. The single-phase nature of the bulk $MgFe_2O_4$ sample was confirmed by X-ray diffraction and Mössbauer spectroscopy.

The X-ray diffraction (XRD) patterns were collected using a URD 6 powder diffractometer (Seifert-FPM, Freiberg, Germany) with Fe Kα radiation. The microstructural characteristics (crystallite size and strains) were obtained from the Rietveld analysis of the XRD data using the PowderCell program.[35] The JCPDS PDF database[8] was utilized for phase identification.

Mössbauer spectra were taken in transmission geometry using a ^{57}Co/Rh γ-ray source. High-field Mössbauer spectra were recorded at an external magnetic field of 5.5 T applied perpendicular to the γ-ray direction. The velocity scale was calibrated relative to ^{57}Fe

(29) Šepelák, V.; Baabe, D.; Litterst, F. J.; Becker, K. D. *J. Appl. Phys.* **2000**, *88*, 5884.
(30) (a) Šepelák, V. *Ann. Chim.* **2002**, *27*, 61. (b) Šepelák, V.; Baabe, D.; Mienert, D.; Litterst, F. J.; Becker, K. D. *Scr. Mater.* **2003**, *48*, 961. (c) Šepelák, V.; Bergmann, I.; Kipp, S.; Becker, K. D. *Z. Anorg. Allg. Chem.* **2005**, *631*, 993.
(31) Pradhan, S. K.; Bid, S.; Gateshki, M.; Petkov, V. *Mater. Chem. Phys.* **2005**, *93*, 224.
(32) (a) Bhowmik, R. N.; Ranganathan, R.; Nagarajan, R.; Ghosh, B.; Kumar, S. *Phys. Rev. B* **2005**, *72*, 094405. (b) Ponpandian, N.; Narayanasamy, A.; Chinnasamy, C. N.; Sivakumar, N.; Greneche, J.-M.; Chattopadhyay, K.; Shinoda, K.; Jeyadevan, B.; Tohji, K. *Appl. Phys. Lett.* **2005**, *86*, 192510. (c) Goya, G. F.; Rechenberg, H. R. *J. Magn. Magn. Mater.* **1999**, *196*−*197*, 191.
(33) (a) Kodama, R. H.; Berkowitz, A. E.; McNiff, E. J.; Foner, S. *J. Appl. Phys.* **1997**, *81*, 5552. (b) Kodama, R. H.; Berkowitz, A. E. *Phys. Rev. B* **1999**, *59*, 6321.
(34) (a) Šepelák, V.; Wilde, L.; Steinike, U.; Becker, K. D. *Mater. Sci. Eng., A* **2004**, *375*−*377*, 865. (b) Šepelák, V.; Baabe, D.; Mienert, D.; Schultze, D.; Krumeich, F.; Litterst, F. J.; Becker, K. D. *J. Magn. Magn. Mater.* **2003**, *257*, 377. (c) Šepelák, V.; Menzel, M.; Becker, K. D.; Krumeich, F. *J. Phys. Chem. B* **2002**, *106*, 6672. (d) Šepelák, V.; Steinike, U.; Uecker, D. C.; Trettin, R.; Wissmann, S.; Becker, K. D. *Solid State Ionics* **1997**, *101*−*103*, 1343.
(35) Kraus, W.; Nolze, G. *PowderCell for Windows*, version 2.4; Federal Institute for Materials Research and Testing: Berlin, Germany, 2000.

in Rh. Recoil spectral analysis software[36] was used for the quantitative evaluation of the Mössbauer spectra. The Voigt-based fitting method provided distributions of hyperfine parameters for multiple sites in a spectrum. A Lorentzian line width of 0.36 mm/s resulting from the fit of the spectrum of a standard bulk $MgFe_2O_4$ was chosen for the fit of the spectrum of mechanosynthesized $MgFe_2O_4$. The degree of inversion, λ, characterizing the distribution of cations over the two nonequivalent cation sublattices provided by the spinel structure, was calculated from the Mössbauer subspectral intensities ($I_{(A)}/I_{[B]} = (f_{(A)}/f_{[B]})(\lambda/(2-\lambda))$), assuming that the ratio of the recoilless fractions is $f_{[B]}/f_{(A)} = 1$ at 3 K and $f_{[B]}/f_{(A)} = 0.94$ at room temperature.[37] The average canting angle, Ψ, was calculated from the ratio of the intensities of lines 2 and 1, I_2/I_1, according to formula $\Psi = 90° - \arcsin\{[3(I_2/I_1)/2]/[1 + 3(I_2/I_1)/4]\}^{1/2}$.[38]

Magnetic measurements were made using a SQUID magnetometer. The morphology of powders and the sizes of individual crystallites were studied using a combined field-emission (scanning) transmission electron microscope (S)TEM (JEOL JEM-2100F) with an ultrahigh-resolution pole piece that provides a point resolution better than 0.19 nm at 200 kV. An energy-dispersive X-ray spectrometer (Oxford Instruments INCA 200 TEM) with an ultrathin window allowed for chemical analysis (distribution of elements) within grains of the mechanosynthesized material. Prior to TEM investigations, powders were crushed in a mortar, dispersed in ethanol, and fixed on a copper-supported carbon film.

Results and Discussion

Figure 1 shows XRD patterns (left) and Mössbauer spectra (right) of the α-Fe_2O_3/MgO mixture milled for various times. For comparison, the XRD pattern and the Mössbauer spectrum of a $MgFe_2O_4$ standard sample (bulk material prepared by the conventional ceramic route) are also presented in Figure 1h.

The XRD pattern of the starting powder (Figure 1a, left) is characterized by sharp diffraction peaks corresponding to crystalline α-Fe_2O_3 (JCPDS PDF 89-0599) and MgO (JCPDS PDF 87-0653).[8] During the early stages of milling (for milling times $t < 2$ h), XRD merely reveals a decrease in the intensity and an associated broadening of the Bragg peaks of the individual oxides. However, for times $t > 2$ h, qualitative changes are observed in the XRD patterns of the milled samples. Clear evidence is observed of diffraction features that correspond to the spinel (220) and (400) diffraction peaks (Figure 1e−g, left). The increased intensity and shift to higher *d*-spacing of the most-intense peak (from $d = 0.2519$ nm to $d = 0.2525$ nm) also suggest the presence of the spinel (311) diffraction peak. After more than 8 h, all peaks detected above the background are due to the $MgFe_2O_4$ phase (JCPDS PDF 88-1943).[8] The Rietveld analysis of the XRD data of the mixture milled for 12 h revealed both an average crystallite size of 8.5(2) nm and the presence of mean strains of $3.2(1) \times 10^{-3}$ in the produced ferrite.

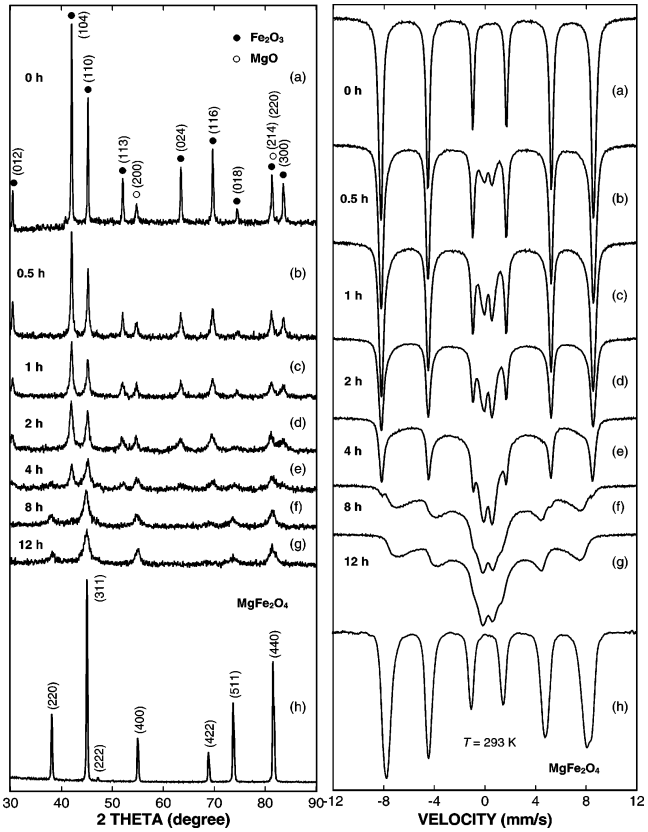

Figure 1. XRD patterns (left) and room-temperature Mössbauer spectra (right) of the α-Fe_2O_3/MgO mixture milled for various times ((a) 0, (b) 0.5, (c) 1, (d) 2, (e) 4, (f) 8, and (g) 12 h) and of (h) bulk $MgFe_2O_4$. Diffraction lines of the reaction precursors and the bulk $MgFe_2O_4$ are denoted by Miller indices.

Formation of the ferrite phase during the high-energy milling of the Fe_2O_3/MgO mixture was also evidenced by Mössbauer spectroscopic measurements (see Figure 1, right). With increasing milling time, a sextet corresponding to α-Fe_2O_3 ($B = 52.26(4)$ T) becomes asymmetric toward the inside of each line, slowly collapses, and is gradually replaced by a central doublet and new broadened sextets. These spectral components can be understood to arise from ^{57}Fe in ferrite particles with relaxation times $\tau < \tau_L$ (dominating superparamagnetic doublet) and $\tau > \tau_L$ (minor sextet structure), where τ_L is the Larmor precession time of the nuclear magnetic moment ($\tau_L \approx 1 \times 10^{-8}$ to 1×10^{-9} s).[39] The broad shape of the Mössbauer spectral lines for mechanosynthesized ferrite, in contrast to relatively narrow magnetically split lines for the bulk material (compare lines g and h in Figure 1, right), provides clear evidence of a wide distribution of magnetic fields acting at the Fe^{3+} nuclei in the nanomaterial.

Figure 2 shows the kinetics of the mechanochemical synthesis as determined by XRD and Mössbauer spectroscopy. In Figure 2a, the normalized intensity of the most-intense (104) XRD peak of α-Fe_2O_3, I_t, is depicted relative to the intensity of this peak in the beginning of the mechanical treatment, I_0. Figure 2b shows the decrease in the intensity of the Mössbauer sextet corresponding to α-Fe_2O_3, I_{sext}, relative to the total spectral intensity, I_{tot},

(36) Lagarec, K.; Rancourt, D. G. *Recoil—Mössbauer Spectral Analysis Software for Windows*, version 1.02; Department of Physics, University of Ottawa: Ottawa, ON, 1998.

(37) Sawatzky, G. A.; Van Der Woude, F.; Morrish, A. H. *Phys. Rev.* **1969**, *183*, 383.

(38) Vandenberghe, R. E.; De Grave, E. In *Mössbauer Spectroscopy Applied to Inorganic Chemistry*; Long, G. J., Grandjean, F., Eds.; Plenum Press: New York, 1989; Vol. 3, p 115.

(39) Mørup, S. In *Mössbauer Spectroscopy Applied to Inorganic Chemistry*; Long, G. J., Ed.; Plenum Press: New York, 1987; Vol. 2, p 89.

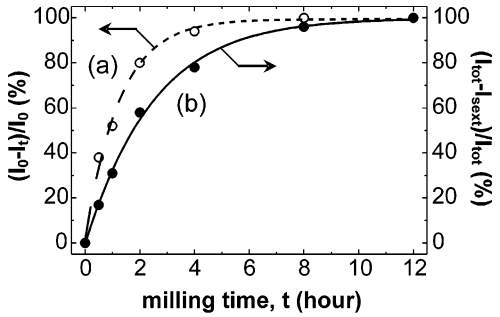

Figure 2. Variations with milling time, *t*, of (a) the normalized intensity of the (104) X-ray diffraction peak of α-Fe_2O_3 and (b) the relative intensity of the Mössbauer sextet corresponding to α-Fe_2O_3.

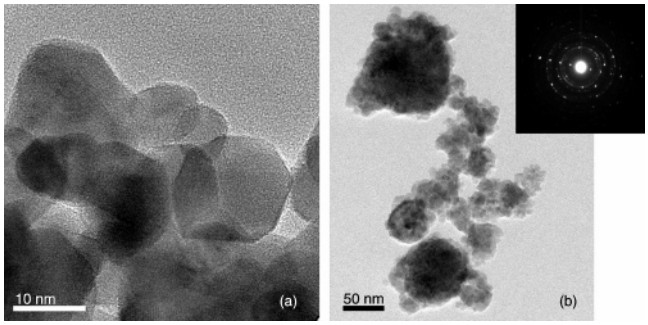

Figure 3. (a) TEM bright-field image of nanoscale mechanosynthesized $MgFe_2O_4$. (b) Nanosized crystallites show a strong tendency for agglomeration; the corresponding SAED pattern is displayed in the inset.

reflecting a gradual conversion of the binary oxides to the ferrite phase during milling. The presence of the α-Fe_2O_3 sextet ($\sim$4% of the total spectral intensity) in the spectrum of the sample milled for 8 h, where no diffraction peak corresponding to α-Fe_2O_3 is registered by XRD (see Figure 1f), gives evidence of the fact that the hyperfine field-sensitive Mössbauer nuclei provide a very sensitive probe for the estimation of the yield of a mechanochemical reaction.

TEM micrographs (Figure 3) show that the mechanosynthesized ferrite consists of crystallites mostly in the 5−15 nm size range, consistent with the average crystallite size determined by XRD. The shape of the majority of the crystallites appears to be spherical (Figure 3a). As shown in Figure 3b, nanoscale crystallites tend to agglomerate because of the dipolar field of each crystallite.[20] Agglomerated crystallites form grains with sizes mostly up to 50 nm. Corresponding selected area electron diffraction (SAED) patterns, displayed in the inset of Figure 3b, show Debye Scherrer rings that fit to a cubic unit cell with a dimension of about 0.839 nm. The discrete diffraction spots of the larger grains indicate the same lattice spacing.

The high-angle annular dark-field (HAADF) micrograph taken in the STEM mode (Figure 4a) shows brightness variations just due to variations in specimen thickness, as do the elemental maps that monitor the local K_α X-ray emission from magnesium, iron, and oxygen (Figure 4b−d). Local elemental concentrations are positively correlated. These findings hint to a homogeneous distribution of elements within agglomerated grains of the mechanosynthesized material. Hereafter, we assume the ideal composition $MgFe_2O_4$.

The low-temperature Mössbauer spectra of both bulk and nanoscale mechanosynthesized $MgFe_2O_4$ are compared in the top and bottom, respectively, of Figure 5a. As clearly shown, the thermal fluctuations are suppressed at 3 K, and the Mössbauer spectrum of nanocrystalline $MgFe_2O_4$ consists of broadened sextets only. Although the influence of superparamagnetic relaxation is counteracted, a determination of the cation distribution in $MgFe_2O_4$ nanoparticles is impossible to make from the low-temperature spectrum (Figure 5a, bottom), because it is difficult to resolve the subspectra or to assign them to the respective lattice sites. This overlapping is known to produce misleading interpretations in some spinel compounds such as $CuFe_2O_4$, where unphysical results are obtained for the iron population if the subspectral intensities are considered.[40] Therefore, in the present case, the iron populations at the (A) and [B] sublattices will be analyzed concurrently with the discussion of in-field Mössbauer data (see below).

To determine both ionic configuration and spin arrangement in mechanosynthesized ferrite nanoparticles, we found it necessary to perform low-temperature Mössbauer measurements in conjunction with large external magnetic fields. In the presence of an external magnetic field (H_{ext}), the effective magnetization of the individual particles is aligned along the field. As a consequence of the antiparallel alignment of the spins of Fe^{3+} cations at (A) and [B] sites in spinel ferrites, the external field adds to the magnetic hyperfine field at (A) sites and subtracts from the hyperfine field at [B] sites.[41] Thus, the use of the large external magnetic fields creates an effective separation of the overlapping subpatterns, thereby allowing for an accurate determination of the cation distribution in ferrites. The high-field Mössbauer spectra with the completely resolved (A) and [B] subspectra for both bulk and nanosized mechanosynthesized $MgFe_2O_4$ taken at 3 K are compared at the top and bottom, respectively, of Figure 5b.

The absorption due to Fe^{3+}(A) in the Mössbauer spectrum of the bulk material was fitted by a single hyperfine pattern. On the other hand, the hyperfine field distribution (HFD) with three hyperfine field components (B(n), $n = 6, 5, 4$) was found as being necessary to the fit of the absorption due to Fe^{3+}[B]. This is consistent with previous Mössbauer studies of bulk $MgFe_2O_4$.[9a,29,42] The Mössbauer parameters resulting from the least-squares fitting of the spectrum of the bulk $MgFe_2O_4$ are given in Table 1. The local magnetic fields experienced by the Fe^{3+}[B] site nuclei (53.97, 52.61, and 51.05 T) arise from the different nearest-neighbor (A) site configurations, namely from $n = 6$, 5, and 4 nearest (A) site magnetic (iron) neighbors, respectively. The degree of inversion of the bulk $MgFe_2O_4$, calculated from the subspectral intensity ratio $I_{(A)}/I_{[B]}$, was found to be $\lambda = 0.90(4)$. The intensity ratio $I_2/I_1 \approx 4/3$ for both (A) and [B] subspectra indicates that the spins are almost completely aligned ($\Psi_{(A)} = 0.4(1)°$, $\Psi_{[B]} = 0.5(4)°$) along the external magnetic field of 5.5 T. Thus, the bulk ferrite exhibits a partly inverse spinel

(40) Evans, B. J.; Hafner, S. *Phys. Lett.* **1966**, *23*, 24.
(41) Long, G. J. *Mössbauer Spectroscopy Applied to Inorganic Chemistry*; Plenum Press: New York, 1987; Vol. 2.
(42) (a) De Grave, E.; Govaert, A.; Chambaere, D.; Robbrecht, G. *Physica B* **1979**, *96*, 103. (b) Hamdeh, H. H.; Xia, Z.; Foehrweiser, R.; McCormick, B. J.; Willey, R. J.; Busca, G. *J. Appl. Phys.* **1994**, *76*, 1135.

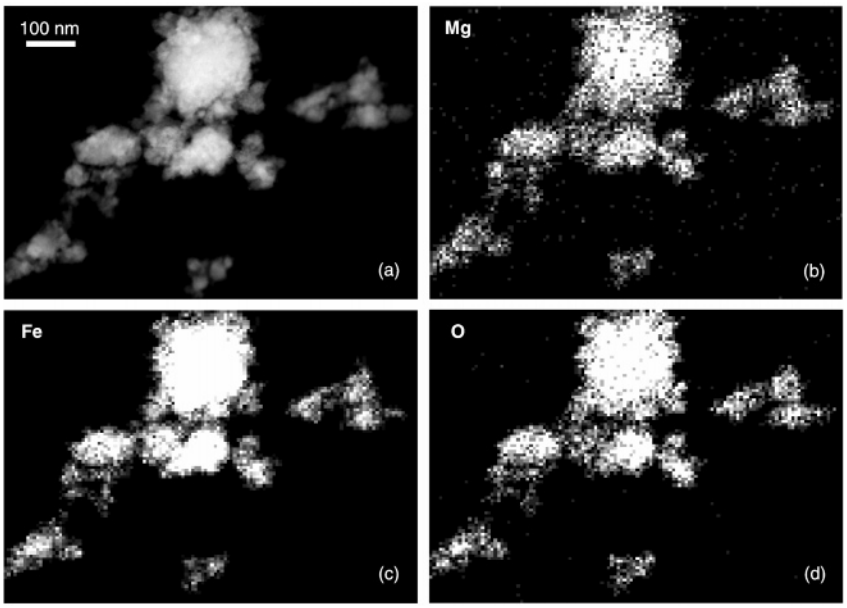

Figure 4. (a) HAADF micrograph of mechanosynthesized $MgFe_2O_4$ taken in the STEM mode. Micrographs showing distribution of the elements (b) magnesium, (c) iron, and (d) oxygen within grains of the mechanosynthesized material. Bright contrasts represent high element concentrations.

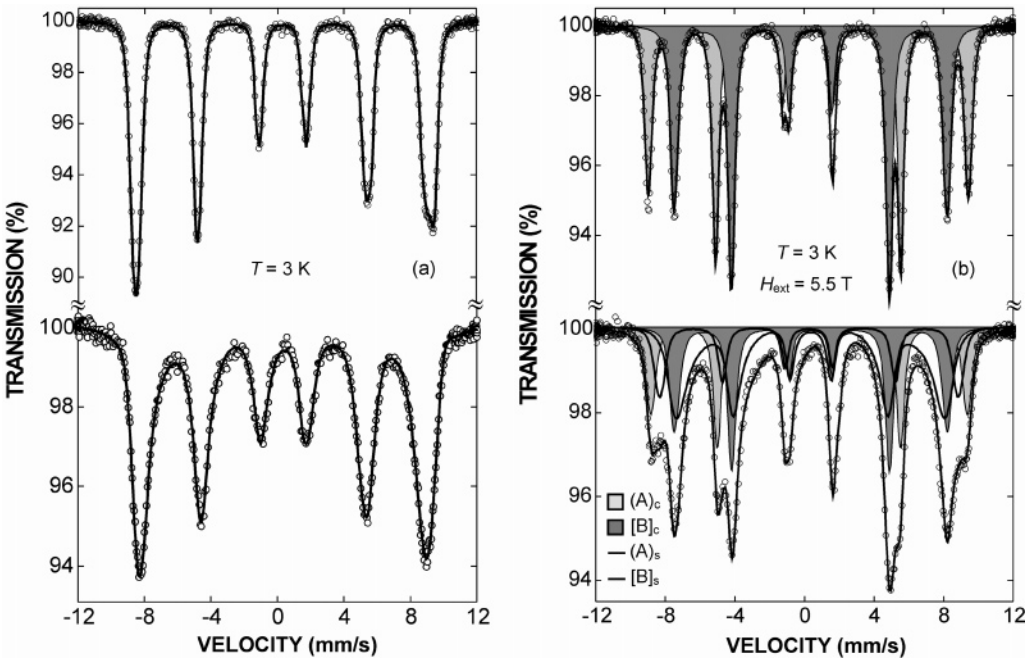

Figure 5. Low-temperature (3 K) Mössbauer spectra of bulk $MgFe_2O_4$ (top) and nanosized mechanosynthesized $MgFe_2O_4$ (bottom) taken at (a) zero applied magnetic field and (b) an external magnetic field of 5.5 T applied perpendicular to the γ-ray direction. $(A)_c$, $[B]_c$ and $(A)_s$, $[B]_s$ denote cation sites of tetrahedral and octahedral coordination in the inner core and the surface shell of $MgFe_2O_4$ nanoparticles, respectively.

structure with a Néel type collinear spin arrangement of $(Mg_{0.10}Fe_{0.90}^{\uparrow})[Mg_{0.90}Fe_{1.10}^{\downarrow}]O_4$.

The high-field Mössbauer spectrum of the mechanosynthesized $MgFe_2O_4$ nanoparticles (Figure 5b, bottom) is well-fitted by assuming an ordered particle core surrounded by disordered grain boundary (surface) regions. This fitting strategy has already been applied in the fitting of the in-field Mössbauer spectra of nanoscale $NiFe_2O_4$[43a] and $CuFe_2O_4$.[43b] Thus, the present Mössbauer data were fitted by a superposition of four subspectra; two accounting for Fe^{3+} nuclei at (A) and [B] sites of the particle core (denoted by $(A)_c$ and $[B]_c$ in Figure 5b and Table 1) and two associated with Fe^{3+} ions at (A) and [B] sites in the surface shell of the nanoparticles (denoted by $(A)_s$ and $[B]_s$, respectively). To separate the surface effects from the bulk effects in the spectrum of mechanosynthesized $MgFe_2O_4$, we assumed that the core of $MgFe_2O_4$ nanoparticles possesses the same structure as the bulk material. Thus, the fit to the spectrum of nanoscale $MgFe_2O_4$ was made by imposing constraints on the Mössbauer parameters of the subspectra corresponding to the particle core (IS, p, B, $I_{(A)c}/I_{[B]c}$, $I_{(A)c2}/I_{(A)c1}$, $I_{[B]c2}/I_{[B]c1}$),

(43) (a) Sousa, E. C.; Sousa, M. H.; Goya, G. F.; Rechenberg, H. R.; Lara, M. C. F. L.; Tourinho, F. A.; Depeyrot, J. *J. Magn. Magn. Mater.* **2004**, *272*−*276*, e1215. (b) Alves, C. R.; Aquino, R.; Sousa, M. H.; Rechenberg, H. R.; Goya, G. F.; Tourinho, F. A.; Depeyrot, J. *J. Metastable Nanocryst. Mater.* **2004**, *20*−*21*, 694.

Table 1. Parameters Obtained by Fitting the High-Field Mössbauer Spectra Taken at 3 K for Bulk $MgFe_2O_4$ and Nanosized Mechanosynthesized $MgFe_2O_4$[a]

subspectrum/ component	IS (mm/s)	p	B (T)	σ (T)	I
		Bulk $MgFe_2O_4$[b]			
(A)	0.25(2)	1.00	50.99(6)	1.10(5)	0.452(1)
[B]	0.36(3)				
B(6)		0.69[c,d]	53.97(4)	0.70(4)	0.378(1)
B(5)		0.26[c,d]	52.61(4)	0.74(6)	0.143(2)
B(4)		0.05[c,d]	51.05(3)	0.83(6)	0.027(4)
		Nanosized $MgFe_2O_4$[e]			
$(A)_c$	0.25[c]	1.00[c]	50.99[c]	1.13(2)	0.230(1)
$[B]_c$	0.36[c]				
$B(6)_c$		0.69[c]	53.97[c]	0.72(4)	0.193(2)
$B(5)_c$		0.26[c]	52.61[c]	0.77(3)	0.073(2)
$B(4)_c$		0.05[c]	51.05[c]	0.86(4)	0.014(1)
$(A)_s$	0.25(1)	1.00	47.71(2)	1.28(3)	0.170(1)
$[B]_s$	0.36(1)				
$B(6)_s$		0.091	53.97[c]	1.23(5)	0.029(1)
$B(5)_s$		0.346	52.61[c]	1.98(7)	0.111(2)
$B(4)_s$		0.338	51.05[c]	3.8(4)	0.108(6)
$B(3)_s$		0.225	45.28(1)	6.1(2)	0.072(1)

[a] (A) = tetrahedrally coordinated site; [B] = octahedrally coordinated site; B(6), B(5), B(4), B(3) = components of the [B] site subspectrum; IS = average isomer shift; p = weight of the component; σ = Gaussian width of the component; I = relative intensity of the component; B = magnetic hyperfine field; $\langle B\rangle$ = average value of the magnetic hyperfine field distribution; λ = degree of inversion; Ψ = average canting angle; $_c$ = inner core of a nanoparticle; $_s$ = surface shell of a nanoparticle; $_1$ = first spectral line; $_2$ = second spectral line. [b] $I_{(A)}/I_{[B]} = 0.824(8)$, $I_{(A)2}/I_{(A)1} = 1.333(2)$, $I_{[B]2}/I_{[B]1} = 1.333(1)$, $\lambda = 0.90(4)$, $\Psi_{(A)} = 0.4(1)°$, $\Psi_{[B]} = 0.5(4)°$, $\langle B\rangle_{[B]} = 53.47(1)$ T. [c] Fixed parameter. [d] The probability that an Fe^{3+}[B] ion possesses n Fe^{3+} and $6 - n$ Mg^{2+} (A) site nearest neighbors, calculated from the binomial distribution for $\lambda \approx 0.9$.[29] [e] $I_{(A)c}/I_{[B]c} = 0.82$[c], $I_{(A)c2}/I_{(A)c1} = I_{[B]c2}/I_{[B]c1} = 4/3$[c] $\rightarrow \lambda_c = 0.90$, $\Psi_{(A)c} = \Psi_{[B]c} = 0°$, $I_{(A)s}/I_{[B]s} = 0.531(3)$, $I_{(A)s2}/I_{(A)s1} = 0.823(6)$, $I_{[B]s2}/I_{[B]s1} = 0.569(2)$, $\lambda_s = 0.69(3)$, $\Psi_{(A)s} = 29.1(1)°$, $\Psi_{[B]s} = 39.3(4)°$, $\langle B\rangle_{[B]s} = 50.75(3)$ T.

such that these parameters were fixed and equal to those obtained from the fit of the spectrum of the bulk material. To allow for a core size distribution of nanoparticles, we freed the Gaussian widths (σ) of the core components $(A)_c$ and $B(n)_c$ ($n = 6, 5, 4$) during the fitting within constraints that were given by the difference in local hyperfine fields. Taking into account that local magnetic fields experienced by Fe^{3+}(A) are virtually independent of the detailed distribution of magnetic ions in the spinel structure,[44] we fitted the absorption due to Fe^{3+} ions at the (A) site of the particle shell by a single hyperfine pattern. To account for the sensitivity of a [B] site ion to the distribution of magnetic ions in its neighborhood,[44] we fitted the absorption due to Fe^{3+} ions at [B] site of the particle shell by a HFD consisting of four components ($B(n)_s$, $n = 6, 5, 4, 3$). It should be noted that a similar fitting approach, comprehending a sensitivity of a particular ion to the distribution of magnetic ions in its neighborhood, has already been applied in the study of the local structure of a disordered spinel.[29] On the basis of the detailed analysis of a broad [B] site HFD, its low-field component was assigned to those Fe^{3+}[B] site nuclei that experience a local surrounding with the reduced number of magnetic neighbors on the nearest (A) sites; for details, see Šepelák et al.[29] In this context, in the present study, the $B(3)_s$ component of the [B] site HFD may be attributed to those Fe^{3+}[B] ions located in the surface region of a $MgFe_2O_4$ nanoparticle that possess 3 nearest (A) site iron neighbors.

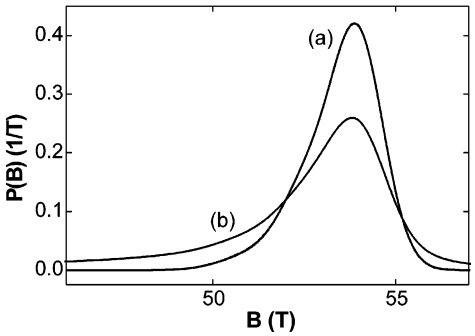

Figure 6. [B] site HFDs derived from the high-field Mössbauer spectra of the (a) bulk and (b) nanosized mechanosynthesized $MgFe_2O_4$. The [B] site HFD of the mechanosynthesized material is a superposition of the core ($[B]_c$) and shell ($[B]_s$) contributions.

Figure 6 compares the [B] site HFDs derived from the high-field Mössbauer spectra of the bulk and mechanosynthesized $MgFe_2O_4$. The hyperfine parameters of (A) and [B] site ferric ions resulting from the least-squares fitting of the spectrum of nanosized $MgFe_2O_4$ are presented in Table 1.

From the relative intensities of sextets, one can easily deduce quantitative information on both the cation distribution and the spin configuration within the $MgFe_2O_4$ nanoparticles. Whereas the core is considered to possess the partly inverse spinel structure ($\lambda_c = 0.90$), the shell region is found to be structurally disordered. The subspectral intensity ratio $I_{(A)s}/I_{[B]s} = 0.531(3)$ indicates that the major feature of the atomic configuration in the shell is a nonequilibrium cation distribution characterized by a reduced fraction of iron cations on (A) sites, $\lambda_s = 0.69(3)$. It should be noted that this value of the degree of inversion corresponds nearly to the random distribution of cations ($\lambda = 2/3$) with maximum configurational entropy.[45] The present observation of the nonuniform cation distribution within $MgFe_2O_4$ nanoparticles by means of Mössbauer spectroscopy is consistent with the results of Rietveld analysis of the XRD data[31] showing that the mechanosynthesized material consists of two spinel phases with different cation distributions.

Another striking feature of the present Mössbauer data is the observed difference between the intensity ratios of spectral lines 2 and 1 for the inner core ($I_{(A)c2}/I_{(A)c1}$, $I_{[B]c2}/I_{[B]c1}$) and the surface region ($I_{(A)s2}/I_{(A)s1}$, $I_{[B]s2}/I_{[B]s1}$), which is a direct indication of a nonuniform spin arrangement within a nanoparticle. Whereas the magnetic moments located at (A) and [B] sites of the particle core are assumed to exhibit a perfect alignment with the external field ($I_{(A)c2}/I_{(A)c1} = I_{[B]c2}I_{[B]c1} = 4/3$), the spins in the shell region are found to be canted. The average canting angles, calculated from the intensity ratios $I_{(A)s2}/I_{(A)s1}$ and $I_{[B]s2}/I_{[B]s1}$, were found to be $\Psi_{(A)s} = 29.1(1)°$ and $\Psi_{[B]s} = 39.3(4)°$, respectively. Thus, the spins located on the two sublattices in the surface regions of mechanosynthesized $MgFe_2O_4$ nanoparticles are found to behave differently under an external field of 5.5 T. This result is also consistent with previous work, where different spin canting in the (A) and [B] sublattices of spinel nanostructures was observed.[32b,46]

(44) Van Der Woude, F.; Sawatzky, G. A. *Phys. Rev. B* **1971**, *4*, 3159.

(45) Sickafus, K. E.; Wills, J. M.; Grimes, N. W. *J. Am. Ceram. Soc.* **1999**, *82*, 3279.

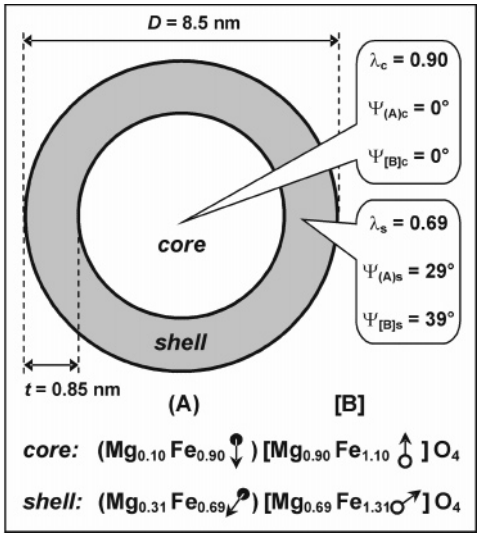

Figure 7. Schematic drawing showing the nonuniform nanostructure of mechanosynthesized $MgFe_2O_4$. The crystal chemical formulas emphasize the spin alignment and the site occupancy at the atomic level within the particle core and shell.

The intensity ratio $(I_{(A)s} + I_{[B]s})/(I_{(A)c} + I_{[B]c} + I_{(A)s} + I_{[B]s}) = 0.490(8)$ indicates that about 50% of the magnetic cations are located in the surface shell of $MgFe_2O_4$ nanoparticles. Assuming a spherical shape of mechanosynthesized nanoparticles and taking their average size as determined by XRD (8.5 nm), we estimated the thickness of the surface shell to be $t \approx 0.85$ nm. This value corresponds to about 4−5 near-surface cation layers and is comparable to the lattice constant of $MgFe_2O_4$ (0.83998 nm).[8] The estimated thickness of the shell is also comparable to that obtained from magnetic measurements on mechanosynthesized $MnFe_2O_4$ nanoparticles (0.91 nm)[21a] and ball-milled $NiFe_2O_4$ (0.88 nm),[47a] but it is smaller than the values estimated from Mössbauer experiments on nanosized $CoFe_2O_4$ (1.0−1.6 nm).[47b] We note that, in general, 1 nm is also a typical thickness of grain boundary regions in nonmagnetic nanocrystalline materials,[48] such as ball-milled $LiNbO_3$, where the grain boundary regions were even shown to be amorphous.[48c] The nonuniform nanostructure of mechanosynthesized $MgFe_2O_4$ is schematically presented in Figure 7.

It is found that the average sublattice magnetic fields experienced by Fe^{3+} ions located in the near-surface layers ($\langle B\rangle_{(A)s} = 47.71(2)$ T, $\langle B\rangle_{[B]s} = 50.75(3)$ T) are reduced in comparison with those acting on iron nuclei in the inner core ($\langle B\rangle_{(A)c} = 50.99(6)$ T, $\langle B\rangle_{[B]c} = 53.47(1)$ T) of $MgFe_2O_4$ nanoparticles. This could be explained by the effect of frustrated superexchange interactions due to the above-described cation disorder and spin canting in the surface regions of nanoparticles. Reduced sublattice magnetic fields have already been reported for nanosized $NiFe_2O_4$ and other ultrafine mechanically alloyed materials.[29,30b,34b] Similar behavior has also been observed in $MgFe_2O_4$ quenched from high temperatures.[49]

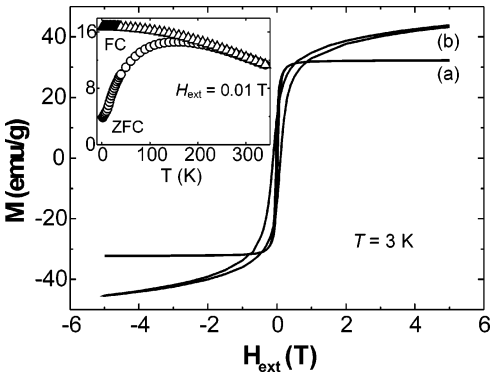

Figure 8. Magnetization hysteresis loops for (a) bulk and (b) nanoscale mechanosynthesized $MgFe_2O_4$ measured at 3 K after field cooling with $H_{ext} = 5$ T. Inset: Zero-field-cooled (ZFC) and field-cooled (FC) magnetization curves for mechanosynthesized $MgFe_2O_4$ taken at $H_{ext} = 0.01$ T.

An interesting observation is that the nanoscale mechanosynthesized $MgFe_2O_4$ exhibits an enhanced magnetization. As can be seen (Figure 8), the magnetization of the mechanosynthesized sample does not saturate even at the maximum field attainable ($H_{ext} = 5$ T). This is in contrast to the magnetic behavior of the bulk $MgFe_2O_4$, whose saturation magnetization reaches the value of $M_{sat} = 33.4$ emu/g. By extrapolating the high-field region of the $M(H_{ext})$ curve to infinite field, we estimated the M_{sat} value of mechanosynthesized $MgFe_2O_4$ to be about 50 emu/g, which represents an enhancement of the saturation magnetization of about 50% (relative to M_{sat} for bulk $MgFe_2O_4$).

Another feature observed is that the field-cooled hysteresis loop of the mechanosynthesized sample is not symmetrical about the origin but is shifted to the left (the shift ΔH_C is about 0.02 T). The asymmetry manifests itself also in the high-field region of the $M(H_{ext})$ curve; M is about +43.8 emu/g at $H_{ext} = 5$ T whereas it is about −45.3 emu/g at the same reversed field. Such an asymmetric hysteresis loop with both horizontal and vertical shifts has been reported for exchange-coupled systems[50] and is explained in terms of exchange coupling between the collinear spins in the core and the canted spins in the shell.[33]

It is also found that the nanoscale mechanosynthesized $MgFe_2O_4$ exhibits an enhanced magnetic hardness, i.e., the coercive field of the mechanosynthesized material ($H_C \approx 0.1$ T) is about 20 times larger than that of the bulk $MgFe_2O_4$ ($H_C \approx 5$ mT). The enhanced coercivity may be attributed to the high volume of the grain boundaries with a nonequilibrium cation distribution and spin canting.[30b] The magnetocrystalline anisotropy, the surface anisotropy, and the shape anisotropy may contribute to such a large coercivity of ultrafine mechanosynthesized particles as well.[50]

The quantitative information on the cation configuration and spin structure, obtained from the analysis of

(46) (a) Helgason, Ö.; Greneche, J.-M.; Berry, F. J.; Mosselmans, F. *J. Phys.: Condens. Matter* **2003**, *15*, 2907. (b) Bhowmik, R. N.; Ranganathan, R.; Sarkar, S.; Bansal, C.; Nagarajan, R. *Phys. Rev. B* **2003**, *68*, 134433. (c) Goya, G. F.; Leite, E. R. *J. Phys.: Condens. Matter* **2003**, *15*, 641.

(47) (a) Zhang, Y. D.; Ge, S. H.; Zhang, H.; Hui, S.; Budnick, J. I.; Hines, W. A.; Yacaman, M. J.; Miki, M. *J. Appl. Phys.* **2004**, *95*, 7130. (b) Haneda, K.; Morrish, A. H. *J. Appl. Phys.* **1988**, *63*, 4258.

(48) (a) Heitjans, P.; Indris, S. *J. Phys.: Condens. Matter* **2003**, *15*, R1257. (b) Heitjans, P.; Indris, S. *J. Mater. Sci.* **2004**, *39*, 5091. (c) Heitjans, P.; Masoud, M.; Feldhoff, A.; Wilkening, M. *Faraday Discuss.* **2006**, DOI: 10.1039/B602887J (in press).

(49) De Grave, E.; Dauwe, C.; Govaert, A.; De Sitter, J. *Phys. Status Solidi B* **1976**, *73*, 527.

(50) Nogués, J.; Sort, J.; Langlais, V.; Skumryev, V.; Suriñach, S.; Muñoz, J. S.; Baró, M. D. *Phys. Rep.* **2005**, *422*, 65.

Mössbauer spectra, is very helpful in the interpretation of the enhanced magnetization of nanocrystalline mechanosynthesized $MgFe_2O_4$. Because Mg^{2+} ions possess no magnetic moment, the total magnetic moment μ in $(Mg_{1-\lambda}Fe_{\lambda}^{\uparrow})[Mg_{\lambda}Fe_{2-\lambda}^{\downarrow}]O_4$ is entirely due to the uncompensated magnetic moments of the ferric ions. Thus, from the degree of inversion and the canting angles, we can calculate the effective magnetic moment (per formula unit) of $MgFe_2O_4$ as

$$\mu = \mu_{[B]} - \mu_{(A)} = (2 - \lambda)\mu_{Fe} \cos \Psi_{[B]} - \lambda\mu_{Fe} \cos \Psi_{(A)}$$

where μ_{Fe} is the magnetic moment of Fe^{3+} ion; $\mu_{Fe} = 5\ \mu_B$ (μ_B is Bohr magneton, $\mu_B = 9.274 \times 10^{-21}$ emu).

In the following, we will calculate the magnetization of mechanosynthesized $MgFe_2O_4$ particles in the framework of the core−shell model. The values $\lambda_c = 0.90$ and $\Psi_{(A)c} = \Psi_{[B]c} = 0°$, characteristic of the core, result in the magnetic moment $\mu_c = 1\ \mu_B$/formula unit. On the other hand, the values $\lambda_s = 0.69$ and $\Psi_{(A)s} = 29°$, $\Psi_{[B]s} = 39°$, characterizing the nonequilibrium cation distribution and spin canting in the grain boundary regions, lead to the effective magnetic moment $\mu_s \approx 2.07\ \mu_B$ per formula unit of $MgFe_2O_4$. Thus, a competition between the effects of spin canting (which generally tends to reduce the magnetic moment) and cation disorder (which brings about an increase in the magnetic moment) theoretically leads to a magnetization of the shell that is approximately 2 times larger than that of the core. Assuming a spherical shape of particles, we can estimate the relative enhancement of the magnetization, ϵ, of mechanosynthesized material using the average particle size determined by XRD ($D = 8.5$ nm) and the thickness of the surface region derived from the Mössbauer data ($t = 0.85$ nm) by applying the following expression

$$\epsilon = \frac{\int_0^{D/2-t} \mu_c 4\pi r^2 dr + \int_{D/2-t}^{D/2} \mu_s 4\pi r^2 dr - \mu_c \frac{4}{3}\pi\left(\frac{D}{2}\right)^3}{\mu_c \frac{4}{3}\pi\left(\frac{D}{2}\right)^3}$$

The theoretically estimated value of $\epsilon \approx 52\%$ is in reasonable agreement with that of about 50% determined from the magnetization measurements (see Figure 8). Thus, the magnetization enhancement of about 50% in mechanosynthesized $MgFe_2O_4$ is attributed to the effect of cation disorder that dominates over the effect of spin canting in the surface shell of nanoparticles. Because of the nearly random distribution of magnetic (Fe^{3+}) cations, the "magnetically active" surface shell exhibits an effective magnetic moment that is approximately 2 times larger than that of the core (or bulk material).

Figure 8 (inset) shows the zero-field cooled (ZFC) curve of mechanosynthesized $MgFe_2O_4$ measured in the temperature range from 2 to 340 K. Above 2 K, the increase with temperature of ZFC curve can be ascribed to the presence of superparamagnetic crystallites, which give rise to a single maximum at about $T_B = 180$ K. This points to a single-stage process of the crystallite blocking.[51] According to Chen et al.[52] this blocking temperature in $MgFe_2O_4$ can be associated with crystallites of average sizes of about 11 nm. It should be noted that the position of the maximum in the ZFC curve is also sensitive to the aggregation level of the particles and to the resulting dipolar magnetic interactions between them.[53] Thus, a good agreement is obtained between the average crystallite size deduced; magnetic measurements are from TEM and XRD. The point at which the ZFC and FC curves start to separate ($T_s \approx 200$ K) is associated with the blocking temperature of bigger crystallites. The relatively small difference between T_B and T_s (∼20 K) demonstrates that the mechanosynthesized $MgFe_2O_4$ possesses a relatively narrow distribution of particle sizes.

The nanostructured $MgFe_2O_4$ prepared by high-energy milling is metastable with respect to structural changes at elevated temperatures. Figure 9 shows the room-temperature Mössbauer spectra of the mechanosynthesized material taken after annealing at various temperatures for 30 min. It was observed that in the temperature range 293−623 K, the shape of the spectra of the nanosized $MgFe_2O_4$ remains unchanged (Figure 9a−c). This demonstrates that the range of the thermal stability of the mechanosynthesized product extends up to 623 K. However, at temperatures above 623 K, a gradual crystallization of the nanoscale $MgFe_2O_4$ powders takes place (see Figure 9d−h). As to be expected, the superparamagnetic doublet component gradually vanishes because of particle growth of the spinel phase. Simultaneously, the sextet structure, typical of the long-range ferrimagnetic state, develops because of the thermally induced changes in the spin configuration. In the temperature range 723−1273 K, the most-apparent change in the spectra is a gradual narrowing of spectral line shapes, implying the disappearance of the broadly distributed hyperfine magnetic fields. The increased intensity of the sextet structure and its shift to higher magnetic hyperfine fields also suggest the formation of an ordered state on heating. The room-temperature Mössbauer spectrum of the annealed sample (at 1273 K for 30 min), measured at an external magnetic field (Figure 9i), consists of two sextets with the parameters $IS_{(A)} = 0.12(8)$ mm/s, $IS_{[B]} = 0.24(5)$ mm/s, $\langle B\rangle_{(A)} = 48.12(3)$ T, and $\langle B\rangle_{[B]} = 50.02(2)$T; values that are well comparable with those of the bulk material.[30b] The quantitative evaluation of the spectral intensities revealed both the collinear spin alignment ($\Psi_{(A)} = 0.4(2)°$, $\Psi_{[B]} = 0.6(2)°$) and the partly inverse spinel structure ($\lambda = 0.89(4)$) of the annealed sample. This indicates that the nonequilibrium cation distribution and the canted spin arrangement resulting from the mechanochemical synthesis route are metastable, i.e., during the annealing process, they relax toward their equilibrium configuration.

The TEM observations of the mechanosynthesized $MgFe_2O_4$ after annealing at various temperatures revealed that the average crystallite size increases with increasing sintering temperature (Figure 9). After the thermal treatment at 1023 K for 30 min, the $MgFe_2O_4$ powder is no more nanocrys-

(51) Yu, S. C.; Song, Y. Y.; Kiss, L. F.; Vincze, I. *J. Magn. Magn. Mater.* **1999**, *203*, 316.

(52) Chen, Q.; Zhang, Z. J. *Appl. Phys. Lett.* **1998**, *73*, 3156.

(53) Dormann, J. L.; Fiorani, D.; Tronc, E. In *Advances in Chemical Physics*; Prigogine, I., Rice, S. A., Eds.; John Wiley and Sons: New York, 1997; Vol. 18.

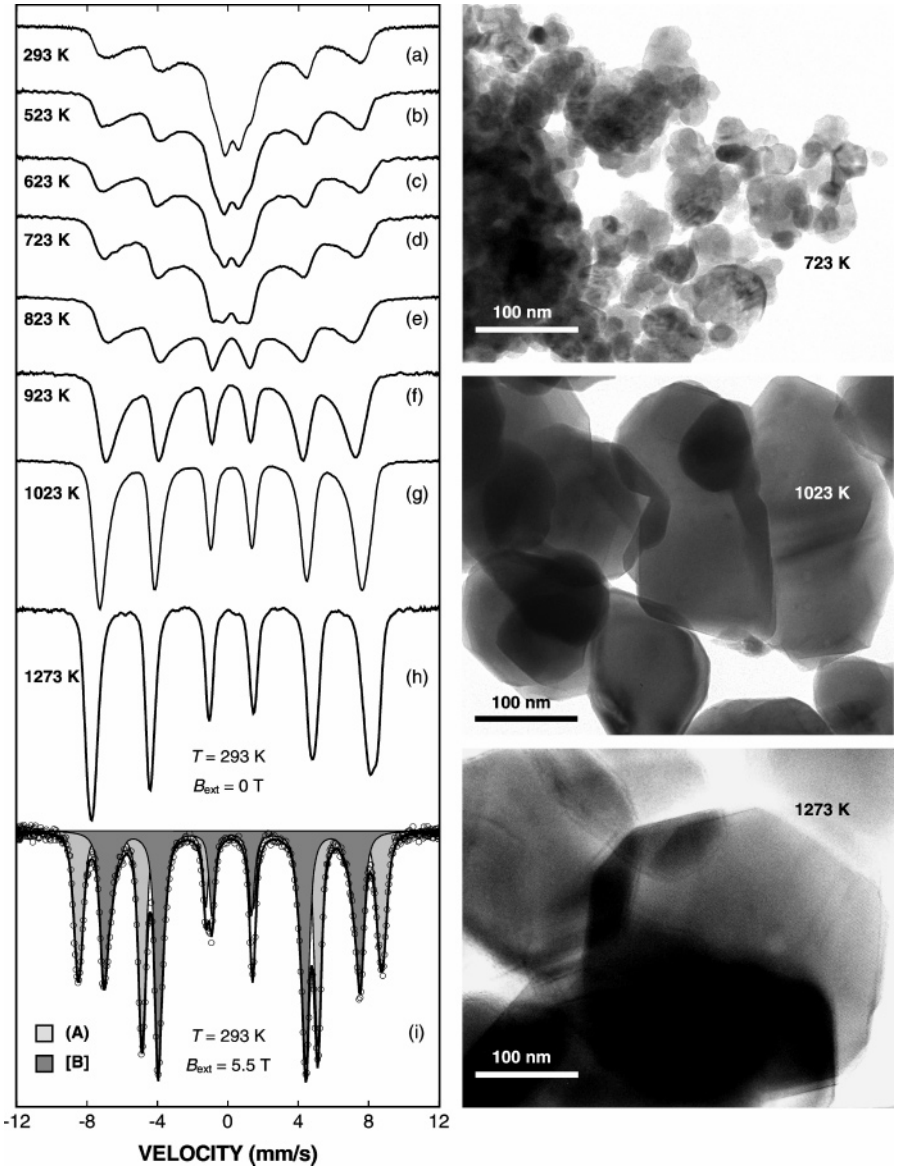

Figure 9. (left) Room-temperature Mössbauer spectra of mechanosynthesized $MgFe_2O_4$ after annealing at various temperatures ((a) 293, (b) 523, (c) 623, (d) 723, (e) 823, (f) 923, (g) 1023, and (h) 1273 K) for 30 min. (i) High-field Mössbauer spectrum of the sample annealed at 1273 K for 30 min, with completely resolved (A) and [B] subspectra. (right) TEM bright-field images of mechanosynthesized $MgFe_2O_4$ after annealing at 723, 1023, and 1273 K (from top to bottom) reveal different crystallite sizes.

talline; its average crystallite size exceeds 100 nm. The annealing at higher temperatures leads to the further growth of crystallites reaching sizes of more than 200 nm. Thus, on heating, the mechanosynthesized $MgFe_2O_4$ has relaxed to a structural and magnetic state that is similar to the bulk one.

Conclusions

Nanosized $MgFe_2O_4$ with an average crystallite size of about 8.5 nm has been synthesized in a one-step mechanochemical route from binary oxide precursors at room temperature. This nonconventional approach offers several advantages over traditional processing routes, including low-temperature solid-state reactions, fewer processing steps, homogeneity of the products, and suitability for the low cost, large-scale production of nanopowders. In this respect, the present work contributes to the search for novel sustainable production routes of functionally tailored nanomaterials.

The comparative in-field Mössbauer study of the bulk and nanosized $MgFe_2O_4$ enables us to separate the surface effects from the bulk effects in mechanosynthesized nanoparticles. It is found that the fraction of magnetic cations that are located in the grain boundary (surface) regions of $MgFe_2O_4$ nanoparticles is about 50%. Assuming a spherical shape of the mechanosynthesized nanoparticles, we estimated the thickness of the surface shell to be about 0.85 nm. This value corresponds to about 4−5 near-surface cation layers and is comparable to the lattice constant of $MgFe_2O_4$. Whereas the core of a $MgFe_2O_4$ nanoparticle exhibits a partly inverse spinel structure ($\lambda_c \approx 0.90$), the atomic configuration in the shell is characterized by the reduced fraction of iron cations on (A) sites ($\lambda_s \approx 0.69$), corresponding to the nearly random distribution of cations. In contrast to the collinear spin alignment in the core of the nanoparticles, the spins located on the (A) and [B] sublattices in the surface shell are canted, and they are found to behave differently under an external

magnetic field ($\Psi_{(A)s} \approx 29°$, $\Psi_{[B]s} \approx 39°$). As a consequence of frustrated superexchange interactions, the average sublattice magnetic fields experienced by Fe^{3+} ions located in the near-surface layers are reduced in comparison with those acting on iron nuclei in the inner core.

It is found that the saturation magnetization of mechanosynthesized $MgFe_2O_4$ reaches the value of $M_{sat} \approx 50$ emu/g, about 50% more than $M_{sat} = 33.4$ emu/g for bulk $MgFe_2O_4$. The theoretical considerations, taking into account the average particle size of mechanosynthesized $MgFe_2O_4$ determined by XRD and the thickness of the surface region derived from the Mössbauer data, lead to a relative magnetization enhancement value of $\epsilon \approx 52\%$, which is in reasonable agreement with that determined from the magnetization measurements. The magnetization enhancement in mechanosynthesized $MgFe_2O_4$ is attributed to the presence of a magnetically active surface shell, whose effective magnetic moment is approximately 2 times larger than that of the bulk material.

The nanostructured $MgFe_2O_4$ prepared by high-energy milling is metastable with respect to structural changes at elevated temperatures. It is found that the range of the thermal stability of the mechanosynthesized product extends up to 623 K. Above this temperature, a gradual crystallization of the nanoscale $MgFe_2O_4$ powders takes place. During the annealing process, the nonequilibrium cation distribution and the canted spin arrangement resulting from the mechanochemical synthesis route relax toward their equilibrium configuration. Thus, on heating to elevated temperatures, the mechanosynthesized $MgFe_2O_4$ relaxes to a structural and magnetic state that is similar to the bulk one.

Acknowledgment. The present work was supported by the Deutsche Forschungsgemeinschaft (DFG). V.Š. thanks the DFG for supporting his work at the Center for Solid State Chemistry and New Materials, University of Hannover, within a Mercator Visiting Professorship. Partial support by the Grant Agency of the Ministry of Education of the Slovak Republic and of the Slovak Academy of Sciences (Grant 2/5146/25) and by the Alexander von Humboldt Foundation is gratefully acknowledged. We are grateful to J. Caro for the opportunity to use the TEM facility.

CM0514894